Whole slide imaging to understand *Candida* biofilm growth and response to antifungals

Maximilian W. D. Raas [1,2], Thiago P. Silva[1], Jhamine C. O. Freitas[3], Lara M. Campos[3], Rodrigo L. Fabri[3], Rossana C.N. Melo[1*]

[1]Laboratory of Cellular Biology, Department of Biology, ICB, Federal University of Juiz de Fora, UFJF, Rua José Lourenço Kelmer, Juiz de Fora, MG, 36036-900, Brazil.

[2]Faculty of Medical Sciences, Radboud University, Geert Grooteplein 10, Nijmegen,6525 GA, The Netherlands

[3]Bioactive Natural Products Laboratory, Department of Biochemistry, Institute of Biological Sciences, Federal University of Juiz de Fora, UFJF, Rua José Lourenço Kelmer, Juiz de Fora, MG, 36036-900, Brazil.

*** Correspondence:** rossana.melo@ufjf.edu.br

Keywords: *Candida spp*., digital microscopy, virtual microscopy; antifungal agents, biofilms, scanning electron microscopy, whole slide imaging.

Abstract

Biofilm formation is a potent factor in the pathogenesis of *Candida* species. The development of new strategies that enable fast and entire visualization of *Candida* biofilms is necessary to better understand their structure and response to antifungals agents. Here, we applied, for the first time, whole slide imaging (WSI), a technique that generates wide-field, high-resolution "digital slides", to study biofilm formation of *Candida* species during normal growth and after treatment with antifungals. Three relevant biofilm-forming *Candida* species (*C. albicans* ATCC 10231*, C. glabrata* ATCC 2001*,* and *C. tropicalis* ATCC 750) were cultivated to grow on glass coverslips in the presence or not of fluconazole or nystatin. Accumulated biofilms on coverslips were then fixed, stained with fluorescent molecular markers for DNA and fungal wall (DAPI or calcofluor-white, respectively), and scanned in both bright-field and fluorescence mode using a digital scanner. WSI enabled clear observation of both size and morphological features of *Candida* biofilms. Quantitative analyses easily detected significant reduction in the surface area covered by biofilms when *Candida* species were exposed to antifungals compared to controls. When the proportions of the whole biofilm areas were compared by using different scanning modalities, there were no significant differences, indicating that the biofilm architecture can be adequately visualized in both bright-field and fluorescence modes and with different fluorophores. High-resolution WSI images also revealed structural aspects of biofilm-composed cells. Fungal cell shape and organization varied from round (isolated yeasts) to elongated cells and WSI morphometric analyses captured significant variations in cell area and cell roundness between *Candida* species. Parallel analyses using scanning electron microscopy confirmed the same observations obtained with WSI in terms of cell morphology, thus demonstrating that WSI resolution is accurate even at single-cell level. Taken together, WSI application allows reliable visualization of *Candida* biofilms from the whole architecture to morphological cell features. Thus, WSI can be a worthy addition to the available microscopic toolset to image and analyse fungal biofilms.

INTRODUCTION

Biofilms are defined as surface-attached, highly resistant, multicellular microbial communities. They are the product of numerous microbes aggregating and some organisms have been observed to wholly merge in this process (Douglas, 2003;Hall-Stoodley et al., 2004). The main constituents of these remarkably resilient structures when produced by yeast-type fungal species are filamentous hyphae, pseudohyphae, yeast-form cells and a self-produced heterogeneous extracellular matrix (Fanning and Mitchell, 2012;Lagree et al., 2018).

Candida biofilm resilience encompasses several aspects. Firstly, they are highly resistant to antifungal agents. Furthermore, when compared to planktonic phase fungal cells, biofilm infections have increased virulence, higher recurrence rates and are known to readily disperse, forming secondary infection sites (Uppuluri et al., 2010;Ramage et al., 2012;Nobile and Johnson, 2015;Del Pozo, 2018). In addition, these pathogenic structures have been shown to suppress immune responses, rendering the host's intrinsic defences ineffective (Xie et al., 2012;Kernien et al., 2017). Taken together, *Candida* biofilms are hard to eradicate and actively promote their survival, procreation and virulence.

As fungal infection disease burden rises alongside increasingly prevailing resistance, research into the fungal biofilm architecture and their response to antifungal agents is becoming more and more pivotal towards successful treatment strategies. A widely used methodology in this research field is scanning electron microscopy (SEM). It provides detailed, ultra-high spatial resolution of the complex three-dimensional (3D) structure that is a biofilm. Other traditional microscopy techniques have been used as well, such as conventional light microscopy and confocal laser scanning microscopy (Lagree et al., 2018), mainly to study local architecture and molecular markers, respectively (Paulitsch et al., 2009). Using these techniques, many meaningful insights concerning architecture and mechanisms of resistance have been acquired.

However, traditional microscopy methods are time-consuming and have their limitations when it comes to complete evaluation of large-scale architecture and biofilm response to antifungal agents, as these techniques focus on a very small section of a biofilm from which the whole structure has to be inducted (Azeredo et al., 2017). Since biofilms are highly complex, multifaceted and heterogeneous (Wimpenny et al., 2000;Kean et al., 2018), this limited view will oftentimes lead to interpretative flaws in understanding the complete structure.

In order to obtain more insights into the cohesion of domains inside a biofilm and to investigate whole biofilm architecture normally growing or following exposure to antifungals, we address here the use of a technique new to the field of biofilm research: whole slide imaging (WSI). This approach allows high-resolution, digital visualization of regular glass slides in their entirety with the use of a digital slide scanner thus generating "digital slides" that offer detailed morphological information and possibility for quantification of multiple morphometric parameters (Webster and Dunstan, 2014;Amaral et al., 2017;Melo et al., 2019). Other WSI benefits are digital storage, easy share ability, the possibility to make annotations on the slide, automated data extraction, remote accessibility and educational purposes (Saco et al., 2016). In the present work, WSI was applied, for the first time, to study biofilm formation of *Candida* species (*C. albicans, C. glabrata,* and *C. tropicalis*) normally growing in cultures and after treatment with antifungals.

MATERIALS & METHODS

Fungal strains

The following yeast strains were used in this study: *Candida albicans* ATCC 10231*, Candida glabrata* ATCC 2001and *Candida tropicalis* ATCC 750. These strains were cultured at 35°C for 48h in Sabouraud agar before all experiments (Campos et al., 2018).

Minimal inhibitory concentration (MIC)

The MIC of fluconazole or nystatin was determined by serial microdilution techniques as proposed before (Khan et al., 2013) in accordance with the Clinical and Laboratory Standards Institute - CLSI-M27 - (CLSI, 2008) using the Brain Heart Infusion (BHI) medium. The stock solution of antifungals was diluted in dimethylsulfoxide (DMSO - final concentration of 1%) to obtain concentrations ranging from 100 to 0.78 µg/mL (*C. glabrata* and *C. tropicalis*) or 160 to 1.25 µg/mL (*C. albicans*). All tests were performed in a volume of 200 µL and plates were incubated at 35ºC for 24h (*C. albicans* and *C. glabrata*) or 48h (*C. tropicalis*) . Controls were established in the BHI medium without the addition of fluconazole or nystatin. The MIC values were calculated as the highest dilution showing complete inhibition of tested strain. All analyses were performed in triplicate and the sterility controls were performed with BHI broth.

Biofilm cultures and antimicrobial treatment

Fungal strains was seeded in Sabouraud Agar media (SDA), incubated (35°C, *C. albicans and C. glabrata:* 24h, C. tropicalis: 48h), and inoculated into a tube with 5 mL of BHI broth and 1% glucose. Then, 500 µL of the inoculated broth were added in microtiter plates (24 wells) containing round glass coverslips (EMS, Hatfield, PA, USA). For each strain, treatment was performed by adding 500 µL of fluconazole (n=4) or nistatin (n=4) at 1 MIC final concentration per well. Wells without addition of any antifungal served as grow controls (n = 4 for each strain). Sterile controls were done in wells with SDA only. *C. albicans* and *C. glabrata* microtiter plates were incubated for 24h at 35°C and *C. tropicalis* plates were incubated for 48h at 35°C.

Biofilm staining

Two classical fluorescent dyes were used for yeast detection, 4′,6-Diamidine-2′-phenylindole dihydrochloride (DAPI) and Calcofluor White (CW). DAPI is a fluorescent dye that binds selectively to double-stranded DNA and CW is a non-specific fluorophore that binds to cellulose and chitin found in cell walls (Hageage and Harrington, 1984;Kapuscinski, 1995). After incubation, supernatants were removed from wells and biofilms on coverslips (n= 48, 12 for each strain) were fixed in freshly prepared formaldehyde solution (final concentration 3.7% in 0,1 M, pH 7,4 PBS) for 30 min. Then, the fixative solution was removed and the coverslips were gently washed with sterile distillate water. Biofilm staining was done by covering the coverslips with 10 µL of DAPI (0.01

µg/mL in PBS, Sigma-Aldrich, USA) or CW stain solution (CW M2R [0.001 g/mL] and evans blue [0.0005 g/mL], Sigma-Aldrich, USA) for 5-10 min in the dark. All steps of fixation and staining were done directly in microtiter plate wells. Next, each coverslip was carefully removed from the plates and attached (side opposite to biofilm) on the surface of a regular glass slide using Entellan mounting medium (Merck) for subsequent scanning as below.

Image acquisition

A WSI scanner is a robotic microscope capable of digitizing an entire glass slide, using software to merge or stitch individually captured images into a composite digital image (Webster and Dunstan, 2014). The images generated through this technology are commonly referred to as a whole slide images, WSIs, whole slide scans or digital slides (Farahani et al., 2015). DAPI and CW stained coverslips from the three *Candida* species were digitally scanned in two different modalities (fluorescence and bright-field) using a 3D Scan Pannoramic Histech scanner (3D HistechKft, Budapest, Hungary) connected to a computer (Fujitsu Technology Solutions GmbH, Munich, Germany). High-resolution images (tiff files uncompressed RGB with 300 DPI) obtained from slides scanned at fluorescence (DAPI and CW) and bright-field modes were acquired using Pannoramic Viewer 1.15.2 SP2 RTM software (3D Histechkft Budapest, Hungary) at different digital magnifications (1-100 X).

Image processing and total biofilm area

Image processing and morphometric analyses of *Candida* biofilms were done using *FIJI* software (National Institutes of Health, Bethesda, MD). First, digital images from CW and DAPI-stained biofilms, scanned at both fluorescent and bright-field modes, were acquired from the entire surface of the glass coverslips at 1- 4x digital magnification and converted to binary (black and white, 0-255) images. Next, images were thresholded to highlight just the biofilm areas through pixel saturation. The threshold processing was done in comparison to the original images to ensure the accuracy of all biofilm areas. Then, quantification of the coverslip areas covered by biofilms was performed by measuring the saturated-pixel areas and establishing the proportions of biofilms.

Scanning electron microscopy

C. albicans, *C. glabrata* and *C. tropicalis* biofilms (fluconazole and nystatin-treated and respective controls) on the surface of coverslips were fixed in freshly prepared aldehydes (1% paraformaldehyde and 1.25% glutaraldehyde) in 0.1 M, pH 7.4 phosphate buffer for 1 h at room temperature and processed as before (Lemos et al., 2018). After post-fixation in 1% osmium tetroxide, the biofilms were washed in phosphate buffer and dehydrated through a graded series of ethanol solutions (30%, 50%, 70%, 90% and twice in 100%) for 15 min at each concentration. Then, samples were critical point dried in carbon dioxide. Subsequently, coverslips were mounted on aluminium holders, sputtered with 5 nm gold and imaged with a double beam scanning electron microscope (Quanta™ 3D FEG, FEI Company, Hillsboro, OR, USA). To study the ultrastructural aspects of the cells, electron micrographs were taken at magnifications of 2,000 – 25,000×.

Cell morphology analyses

The assessment of *Candida* cellular morphology in biofilms was done by both WSI (cells stained with CW) and SEM. Scanned images (40-100× digital magnification, RGB or grayscale) from CW stained biofilms and electron micrographs (magnifications of 5,000-25,000×) were analyzed using FIJI software (National Institutes of Health, Bethesda, MD). Cell area and roundness were analyzed in a total of 321 yeast cells as shown in Table 1. The roundness was automatically calculated by 4*area/(π*major_axis^2), with 1.0 indicating a perfect circle and larger values indicating oblong cells.

Table 1: Number of *C. albicans*, *C. glabrata* and *C. tropicalis* cells analyzed by WSI and SEM.

Experimental Groups	*C. albicans*		*C. glabrata*		*C. tropicalis*	
	WSI	SEM	WSI	SEM	WSI	SEM
Growth control (GC)	41 cells	50 cells	46 cells	40 cells	34 cells	33 cells
Fluconazole	40 cells	50 cells	36 cells	40 cells	21 cells	35 cells
Nystatin	34 cells	44 cells	41 cells	28 cells	39 cells	28 cells
Total (n)	115	144	123	108	94	96

Statistical Analysis

Data from biofilm areas and cell morphology were compared using Anova followed by Tukey's comparison test, or Kruskal-Wallis test. The relationship between biofilm areas acquired by different scan modalities (bright-field and fluorescence [DAPI or CW]) was determined using least square regression. All statistics was performed using GraphPad Prism version 8.00 for Windows (GraphPad Software, La Jolla California, www.graphpad.com), considering $P < 0.05$ as a threshold level for acceptance.

RESULTS

MIC analyses

The MIC assay indicates susceptibility or resistance of fungal strains. First, we evaluated the MIC for all fungal strains in response to fluconazole or nystatin as presented in Table 2.

Table 2: MIC values for fluconazole and nystatin for the different fungal strains

Candida species	MIC Fluconazole (μg/mL)	MIC Nystatin (μg/mL)
C. albicans	>64	2.5
C. glabrata	50	12.5
C. tropicalis	12.5	12.5

Strains are considered susceptible to fluconazole if their MIC is <64 μg/mL. Subsequently, resistance is defined at having a MIC of ≥64 μg/mL (Ghannoum and Rice, 1999;Pfaller et al., 2006). For nystatin, the breakpoint is defined as a MIC of <16 μg/mL (=susceptibility) and ≥16 μg/mL (=resistance) (Kuriyama et al., 2005). Given this information, *C. albicans* strain can be considered resistant to fluconazole and susceptible to nystatin. The other strains (*C. glabrata* and *C. tropicalis)* were considered susceptible to both fluconazole and nystatin. Thus, for resistant *C. albicans*, the breakpoint value for resistance was applied for all tests.

Assessment of biofilms with WSI

Having established the MICs for all strains, cultures of *Candida* species were grown on the surface of round glass coverslips within plates with or without the presence of antifungals agents (Figure 1). After the incubation period, coverslips were stained with two different fluorophores [DAPI (n=24) and CW (n=24)], affixed on glass slides and scanned in a digital scanner with three different WSI strategies: bright-field (BF) mode (all slides, n=48), fluorescence mode after DAPI staining (n=24) and fluorescence mode after CW staining (n=24) (Figure 1A-D). Thus, a total of 96 high-resolution virtual images covering the total biofilm area were acquired for subsequent viewing and morphometric analyses using software (Figure 1E, F). Each virtual image represents an entire glass coverslip/slide (Figure 1). Comparisons were drawn between BF and fluorescence modalities to explore their accuracy and reliability.

WSI enables reliable quantification of biofilm development

The biofilm surface area is a reliable measure of the fungal ability to attach to a surface and proliferate (CLSI, 2008). WSI showed to be a very useful tool to examine large-scale biofilms of *Candida* species, both in normal growth and in the presence of antifungal agents. In all growth control (GC) samples, biofilms covered most surfaces of the coverslips, as shown below for each species. Of note, in general, inhibitory antifungal exposure (1 MIC) was able to effectively accomplish very high levels of inhibition of biofilm formation. The antifungal breakpoint value for resistance applied to fluconazole-resistant *C. albicans,* showed that the amount of biofilm formed was found to be significantly affected. These findings are in line with the expectations, as described below.

C. albicans

Compared to the control group (Figure 1A-C), fluconazole exposure caused widespread dispersion of the resistant *C. albicans* across the coverslips (Figures 2D-F). Nystatin-exposed *C. albicans* cells were not able to establish any meaningful biofilm on the coverslip (Figures 2G-I). WSI quantitative analyses considering all WSI modalities showed a significant decrease of biofilm-covered area in the presence of antifungals (Figure 2J; $P<0.0001$). When the extent of biofilms acquired with different WSI modalities were compared, there were no significant differences among all three strategies (Figure 2K; $P>0.999$ for all). It should be noted that, despite the *C. albicans'* resistance to fluconazole, there was a significant decrease in the amount of biofilm formed in the presence of fluconazole at breaking point value for resistance (BF, DAPI, CW: $P<0.0001$). However, the amount of biofilm in this condition was significantly larger than the amount formed in presence of 1 MIC nystatin (BF: $P=0.010$, DAPI: $P=0.342$*, CW:* $P=0.003$) as seen in Figure 2K.

C. glabrata

This *Candida* strain was susceptible to both antifungals. This was clearly demonstrated by the extent of formed biofilms. While in the control group (Figure 2A-C), biofilms occupied most of the coverslip surface, treated samples displayed very low levels of biofilm coverage (Figure 3D-I). Measurements of the biofilm-covered areas taken in all scanning modalities confirmed the drastic decrease in the amount of biofilm formed following exposure to antifungals compared to the control group (Figure 3J; $P<0.0001$). As shown for *C. albicans*, individual WSI modes did not affect visualization of biofilm areas (Figure 3K; $P>0.999$ for all). In each WSI modality, a significant decrease in the proportion of biofilm coverage was observed after fluconazole or nystatin treatments (BF, DAPI, CW: $P<0.0001$ for each).

C. tropicalis

This *Candida* strain showed no resistance during the MIC experiments. Accordingly, compared to the control group (Figure 3A-C), large decreases in the biofilm extent were observed by *C. tropicalis* in the presence of fluconazole or nystatin (Figure 4D-I; $P<0.0001$). Quantitative analyses considering all WSI modes confirmed a significant reduction in the proportion of biofilm-covered areas after both treatments in comparison to the control group (Figure 4J; $P<0.0001$). Each individual WSI mode also detected significant reduction of the biofilm areas in response to antifungals (BF, DAPI, CW: $P<0.0001$).

Of note, application of additional statistical method (regression analysis) for all *Candida* species and treatments demonstrated that the total surface area of biofilms measured under different WSI modalities were correlated thus demonstrating that the biofilm areas can be reliably detected by BF and fluorescence modes (Supplementary Figure S1).

WSI is a useful tool to assess biofilm structure

By measuring the biofilm areas visualized with WSI, we noticed that additional information on structural aspects of *Candida* biofilms could be obtained from the high-resolution images when seen in high magnification. Thus, WSI revealed the organization of the biofilms for the different *Candida* species (Figure 5). *C. albicans* generally clustered in one large and highly dense biofilm with channel-like structures flowing through them (Figure 5A, B). This aspect was not seen for *C. glabrata* (Figure 5C, D) *and C. tropicalis* (Figure 5E, F) biofilms, which appeared as a less dense structure with typical meshwork aspect. While *C. glabrata* biofilm is characterized by thin filamentous stretches of relatively small fungal cells surrounding an empty, almost round opening (Figure 5 C, D), *C. tropicalis* (Figure 5E, F) forms a meshwork with thicker septa with a slightly lesser cell density. These septa also include circular openings of their own creating an intricate pattern presented.

WSI reveals biofilm morphology at single-cell level

WSI revealed not only the species-specific organization of the biofilms (Figure 5), but also morphological aspects (cell shape) of individual cells. High-resolution WSI analyses of biofilms stained with CW, which enables visualization of the cell surface (cell wall), enabled the observation of round and elongated cells in both RGB (Figure 6A-C) and grayscale (Figure 6D-F).

To evaluate the accuracy of biofilm-composed cell shapes, we next prepared additional samples of *Candida* species growing in normal conditions to SEM, a technique considered a "golden standard" to study cell morphology in biofilms (Azeredo et al., 2017). SEM (Figure 7G-I) showed in 3D the same morphological aspects depicted by WSI images (Figure 7A-F). We then applied quantitative analyses to evaluate cell area and cell roundness in the images acquired by both WSI and SEM. These two parameters are considered relevant to study yeast cell shapes (Lee et al., 2011;Liu et al., 2011;Wang and Lin, 2012;Bougen-Zhukov et al., 2017). In all cases, the data for cell morphometric assessment with WSI did not differ from the data acquired with SEM (P >0.90 for all), indicating that the resolution of WSI is accurate at this level and for this purpose.

Remarkably, morphometric analyses revealed that the area of individual cells in the biofilm significantly varies depending on the *Candida* species and that this variation can be detected by both WSI and SEM (Figure 6J). Cell roundness analyses, done with both WSI and SEM images, revealed significant differences when *C. albicans* was compared to *C. glabrata* (Figure 6K, $P = 0.01$).

Discussion

Most fungal pathogens exist as adhered cells to surfaces within a well-organized biofilm ecosystem and not as free-floating organisms. However, the architecture of fungal biofilms is not fully understood. In the present study, we explore the use of WSI as an approach for large-scale imaging of *Candida* biofilms. One of the advantages of WSI is that it produces images with high resolution and, at the same time, with a wide field of observation. Here, WSI application facilitated comprehensive visualization of *Candida* biofilms both in natural growth and in presence of antifungal agents. Moreover, WSI combined with computational methods enabled fast quantification of the adhesion extent of *Candida* biofilms.

Our data show that inhibitory concentrations of antifungal agents applied to planktonic fungi can effectively inhibit the formation of biofilms. Moreover, breaking point concentrations for resistance applied to a *C. albican*s resistant-strain may lead to significant decreases in the amount of biofilm formed by this strain within a 24h period. Both biofilm formation and biofilm reduction after treatment with antifungals were properly detected by WSI. Our findings demonstrated no variation in the reduction of area covered by biofilms after treatments when WSI modalities were compared. Thus, WSI can be a valuable tool to accurately test biofilm responses to antifungals regardless if the images are acquired under bright-field or fluorescence (DAPI and CW) WSI modes, indicating reliability of WSI settings.

Remarkably, not only the extent but also structural aspects of biofilms were captured by WSI. This approach revealed, for example, that *C. albicans* form complex and highly organized channel-like openings inside its biofilm that, to our knowledge, have been scarcely studied. As these channels are important size-determining aspects of a biofilm due to their facilitation of nutrient-flow (Ramage et al., 2001), WSI can be particularly useful to address future studies focused on these structures.

Since WSI delivers high-resolution images, it also offers the possibility to perform high amount of analyses at the single-cell level, thus extracting more biologically significant cellular information. This has been the case of WSI applications to pathological analyses of biopsies in different fields. For example, in the field of liver pathology and biology, WSI has been extensively used for different purposes, such as to understand cellular diversity of hepatic progenitors, scoring of inflammatory cells and identification of specific hepatocarcinoma cell alterations [reviewed in (Melo et al., 2019)].

Here, we expand the application of WSI to understand morphological aspects of *Candida* species within a biofilm. Our data showed that WSI is a reliable tool for evaluation of the cell area and cell roundness as addressed by fluorescence WSI modality. Cellular area and roundness are important parameters related to environmental conditions and can even reflect specific yeast molecular features, such as cell cycle phase, genetic expression (phenotypic characteristics) or virulence (Lee et al., 2011;Liu et al., 2011;Wang and Lin, 2012;Bougen-Zhukov et al., 2017). Our quantitative analyses revealed that these parameters can vary among *Candida* species (Figure 6) and therefore WSI can be beneficial to understand cell behavior within a biofilm. Yet, the morphometric data acquired from WSI scans showed no significant differences from data extracted from SEM, a technique widely used for biofilm studies and accepted as particularly accurate at high resolution (Azeredo et al., 2017).

WSI was also found to be a practical approach for imaging *Candida* biofilms. The digitalization is fully automated, and wide-field images can be stored. Complete slide scanning means that every slide can be entirely revisited at any point allowing more detailed assessment as the analyses are not confined to limited fields-of-view captured with a regular light microscope fitted with a camera. Easy accessibility, shareability and storage allowed us to explore and quantify data from the scans using adequate software. The possibility to make annotations on slides was also very convenient, since this procedure highlights specific sections of the scan thus facilitating discussion, including remote access. On the other hand, by our experience, WSI does have some limitations for biofilm studies, especially when using unfixed biofilms stained with fluorochromes, which does not allow adequate focus. The scanning process of fluorescent samples also takes more time compared to bright-field modality, but this issue has been addressed with new generation of scanners.

Finally, the present work, to our knowledge is the first to use WSI to study fungal biofilms with perspective of applications not only to *Candida* biofilm investigations but also to other fungal biofilms. A recent work has likewise demonstrated that WSI can be useful to study bacterial biofilms. This technique enabled to examine biofilms produced by *Salmonella enterica* strains after treatment with plant extracts with potential anti-bacterial activity (Campos et al., 2019). Moreover, WSI was used to investigate antibiotic resistance at single-bacterium level (Song et al., 2019). In conclusion, WSI has proved to be a powerful tool in delivering an accurate, high-resolution and full-length view of *Candida* biofilms and therefore can be a worthy and efficient addition to the available microscopic toolset to image and analyse fungal biofilms.

Ethical approval and consent to participate

Not applicable

Adherence to national and international regulations

Not applicable

Consent for publication

Not applicable

Availability of data and materials

The datasets used and/or analysed during the current study are available from the corresponding author on request.

Competing interests

The authors declare that they have no competing interests.

Funding

This work was supported in part by Conselho Nacional de Desenvolvimento Científico e Tecnológico (CNPq, Brazil), Grants 309734/2018-5 and 434914/2018-5 for RCNM and Fundação de Amparo a Pesquisa do Estado de Minas Gerais (FAPEMIG, Brazil).

Author's contributions

RM provided the study design, study mentorship and critical editing of the manuscript. MR, TS and RF contributed to the study design. MR and TS performed experiments and acquired and analyzed the data. JF and LC performed cultures. All authors contributed in part to writing and editing the manuscript and approved the final version.

Acknowledgements

The authors would like to thank Andreia Alvim for discussions as well as suggestions made during scanning electron microscopy. We thank the UFMG Microscopy Center (Belo Horizonte, Brazil) for technical support in sample preparation and image acquisition for scanning electron microscopy.

References

Amaral, K.B., Silva, T.P., Dias, F.F., Malta, K.K., Rosa, F.M., Costa-Neto, S.F., Gentile, R., and Melo, R.C.N. (2017). Histological assessment of granulomas in natural and experimental Schistosoma mansoni infections using whole slide imaging. *PLoS One* 12**,** e0184696. doi: 10.1371/journal.pone.0184696.

Azeredo, J., Azevedo, N.F., Briandet, R., Cerca, N., Coenye, T., Costa, A.R., Desvaux, M., Di Bonaventura, G., Hebraud, M., Jaglic, Z., Kacaniova, M., Knochel, S., Lourenco, A., Mergulhao, F., Meyer, R.L., Nychas, G., Simoes, M., Tresse, O., and Sternberg, C. (2017). Critical review on biofilm methods. *Crit Rev Microbiol* 43**,** 313-351. doi: 10.1080/1040841x.2016.1208146.

Bougen-Zhukov, N., Loh, S.Y., Lee, H.K., and Loo, L.H. (2017). Large-scale image-based screening and profiling of cellular phenotypes. *Cytometry A* 91**,** 115-125. doi: 10.1002/cyto.a.22909.

Campos, L.M., Lemos, A.S., Silva, T.P., Oliveira, L.G., Nascimento, A.L.R., Carvalho, J.J., de Moraes, A.C., Rocha, V.N., Aguiar, J.A., Scio, E., Apolônio, A.C., Melo, R.C.N., and Fabri, R. (2019). Mitracarpus frigidus is active against Salmonella enterica species including the biofilm form. *Ind Crops Prod* 141**,** 111793.

Campos, L.M., Melo, L., Lemos, A.S.O., Guedes, M.C.M.R., Silva, T.P., Figueiredo, G.F., Reis Junior, F.B., Rocha, V.N., Melo, R.C.N., Araújo, M.G.F., Apolonio, A.C.M., Scio, E., and Fabre, A. (2018). Mitracarpus frigidus: A promising antifungal in the treatment of vulvovaginal candidiasis. *Ind Crops Prod* 12**,** 731-739.

CLSI (2008). "Clinical and Laboratory Standards Institute. Reference method for broth dilution antifungal susceptibility testing of yeasts; approved standard", in: *CLSI document M27-A3 and Supplement S.* (Wayne, PA, USA).

Del Pozo, J.L. (2018). Biofilm-related disease. *Expert Rev Anti Infect Ther* 16**,** 51-65. doi: 10.1080/14787210.2018.1417036.

Douglas, L.J. (2003). *Candida* biofilms and their role in infection. *Trends Microbiol* 11**,** 30-36.

Fanning, S., and Mitchell, A.P. (2012). Fungal biofilms. *PLoS Pathog* 8**,** e1002585. doi: 10.1371/journal.ppat.1002585.

Farahani, N., Parwani, A.V., and Pantanowitz, L. (2015). Whole slide imaging in pathology: advantages, limitations, and emerging perspectives. *Pathol Lab Med Int* 7**,** 23-33.

Ghannoum, M.A., and Rice, L.B. (1999). Antifungal agents: mode of action, mechanisms of resistance, and correlation of these mechanisms with bacterial resistance. *Clin Microbiol Rev* 12**,** 501-517.

Hageage, G.J., and Harrington, B.J. (1984). Use of calcofluor white in clinical mycology. *Laboratory Medicine* 15**,** 109-112.

Hall-Stoodley, L., Costerton, J.W., and Stoodley, P. (2004). Bacterial biofilms: from the natural environment to infectious diseases. *Nat Rev Microbiol* 2**,** 95-108. doi: 10.1038/nrmicro821.

Kapuscinski, J. (1995). DAPI: a DNA-specific fluorescent probe. *Biotech Histochem* 70**,** 220-233. doi: 10.3109/10520299509108199.

Kean, R., Delaney, C., Rajendran, R., Sherry, L., Metcalfe, R., Thomas, R., McLean, W., Williams, C., and Ramage, G. (2018). Gaining Insights from *Candida* Biofilm Heterogeneity: One Size Does Not Fit All. *J Fungi (Basel)* 4. doi: 10.3390/jof4010012.

Kernien, J.F., Snarr, B.D., Sheppard, D.C., and Nett, J.E. (2017). The Interface between Fungal Biofilms and Innate Immunity. *Front Immunol* 8**,** 1968. doi: 10.3389/fimmu.2017.01968.

Khan, M.S.A., Ahmad, I., and Cameotra, S.S. (2013). Phenyl aldehyde and propanoids exert multiple sites of action towards cell membrane and cell wall targeting ergosterol in *Candi*da *albicans*. *Amb Express* 3**,** 54. doi: https://doi.org/10.1186/2191-0855-3-54.

Kuriyama, T., Williams, D.W., Bagg, J., Coulter, W.A., Ready, D., and Lewis, M.A. (2005). In vitro susceptibility of oral *Candida* to seven antifungal agents. *Oral Microbiol Immunol* 20**,** 349-353. doi: 10.1111/j.1399-302X.2005.00236.x.

Lagree, K., Desai, J.V., Finkel, J.S., and Lanni, F. (2018). Microscopy of fungal biofilms. *Curr Opin Microbiol* 43**,** 100-107. doi: 10.1016/j.mib.2017.12.008.

Lee, H.N., Magwene, P.M., and Brem, R.B. (2011). Natural variation in CDC28 underlies morphological phenotypes in an environmental yeast isolate. *Genetics* 188**,** 723-730. doi: 10.1534/genetics.111.128819.

Lemos, A.S.O., Campos, L.M., Melo, L., Guedes, M., Oliveira, L.G., Silva, T.P., Melo, R.C.N., Rocha, V.N., Aguiar, J.A.K., Apolonio, A.C.M., Scio, E., and Fabri, R.L. (2018). Antibacterial and Antibiofilm Activities of Psychorubrin, a Pyranonaphthoquinone Isolated From Mitracarpus frigidus (Rubiaceae). *Front Microbiol* 9**,** 724. doi: 10.3389/fmicb.2018.00724.

Liu, Y., Aubrey, W., Martin, K., Sparkes, A., Lu, C., and King, R.D. (2011). The analysis of yeast cell morphology features in exponential and stationary Phase. *J Biol Systems* 19**,** 561-575.

Melo, R.C.N., Raas, M.W.D., Palazzi, C., Neves, V.H., Malta, K.K., and Silva, T.P. (2019). Whole Slide Imaging and Its Applications to Histopathological Studies of Liver Disorders. *Front Med (Lausanne)* 6**,** 310. doi: 10.3389/fmed.2019.00310.

Nobile, C.J., and Johnson, A.D. (2015). *Candida albicans* Biofilms and Human Disease. *Annu Rev Microbiol* 69**,** 71-92. doi: 10.1146/annurev-micro-091014-104330.

Paulitsch, A.H., Willinger, B., Zsalatz, B., Stabentheiner, E., Marth, E., and Buzina, W. (2009). In-vivo *Candida* biofilms in scanning electron microscopy. *Med Mycol* 47**,** 690-696. doi: 10.3109/13693780802635237.

Pfaller, M.A., Diekema, D.J., and Sheehan, D.J. (2006). Interpretive breakpoints for fluconazole and *Candida* revisited: a blueprint for the future of antifungal susceptibility testing. *Clin Microbiol Rev* 19**,** 435-447. doi: 10.1128/cmr.19.2.435-447.2006.

Ramage, G., Rajendran, R., Sherry, L., and Williams, C. (2012). Fungal biofilm resistance. *Int J Microbiol* 2012**,** 528521. doi: 10.1155/2012/528521.

Ramage, G., Vandewalle, K., Wickes, B.L., and Lopez-Ribot, J.L. (2001). Characteristics of biofilm formation by *Candida albicans*. *Rev Iberoam Micol* 18**,** 163-170.

Saco, A., Bombi, J.A., Garcia, A., Ramirez, J., and Ordi, J. (2016). Current Status of Whole-Slide Imaging in Education. *Pathobiology* 83**,** 79-88. doi: 10.1159/000442391.

Song, D., Liu, H., Ji, H., and Lei, Y. (2019). Whole Slide Imaging for High-Throughput Sensing Antibiotic Resistance at Single-Bacterium Level and Its Application to Rapid Antibiotic Susceptibility Testing. *Molecules* 24**,** 2441.

Uppuluri, P., Chaturvedi, A.K., Srinivasan, A., Banerjee, M., Ramasubramaniam, A.K., Kohler, J.R., Kadosh, D., and Lopez-Ribot, J.L. (2010). Dispersion as an important step in the *Candida albicans* biofilm developmental cycle. *PLoS Pathog* 6**,** e1000828. doi: 10.1371/journal.ppat.1000828.

Wang, L., and Lin, X. (2012). Morphogenesis in fungal pathogenicity: shape, size, and surface. *PLoS Pathog* 8**,** e1003027. doi: 10.1371/journal.ppat.1003027.

Webster, J.D., and Dunstan, R.W. (2014). Whole-slide imaging and automated image analysis: considerations and opportunities in the practice of pathology. *Vet Pathol* 51**,** 211-223. doi: 10.1177/0300985813503570.

Wimpenny, J., Manz, W., and Szewzyk, U. (2000). Heterogeneity in biofilms. *FEMS Microbiol Rev* 24**,** 661-671. doi: 10.1111/j.1574-6976.2000.tb00565.x.

Xie, Z., Thompson, A., Sobue, T., Kashleva, H., Xu, H., Vasilakos, J., and Dongari-Bagtzoglou, A. (2012). *Candida albicans* biofilms do not trigger reactive oxygen species and evade neutrophil killing. *J Infect Dis* 206**,** 1936-1945. doi: 10.1093/infdis/jis607.

Legends

Figure 1 - Assessment of biofilms with WSI. (A) Round glass coverslips were used for growing biofilms in cultures. (B) Cultures of *C. albicans*, *C. glabrata* and *C. tropicalis* were cultivated in microtiter plates with or without the presence of antifungals agents and developed biofilms on the surface of coverslips were stained with two different fluorophores [DAPI and Calcofluor-white (CW); n=4/group/each staining]. (C) Stained coverslips were affixed on regular glass slides using Entellan mounting medium. (D) Glass slides with coverslips were scanned in a digital scanner (3D HistechKft, Budapest, Hungary) in two different modalities (bright-field and fluorescence). (E) High-resolution images were acquired using Pannoramic Viewer 1.15.2 SP2 RTM software (3D Histechkft Budapest, Hungary). (F) Virtual images (RGB) were converted to 8-bit (black and white) and thresholded for morphometric analyses using FIJI software.

Figure 2 - Evaluation of *C. albicans* biofilm growth with WSI. (A-I) Virtual images of biofilms growing at the surface of coverslips in the control group (A-C) and after antifungal treatments (D-I) acquired with different scans strategies. In (J), the biofilm-covered areas were quantitated for each group considering all scan modes. (K) The proportion of biofilm coverage is shown per each scan mode. Significant (asterisks) and non-significant (NS) differences are indicated when groups were compared. Scale bar = 1,400 μm

Figure 3 - Evaluation of *C. glabrata* biofilm growth with WSI. (A-I) Virtual images of biofilms growing at the surface of coverslips in the control group (A-C) and after antifungal treatments (D-I) acquired with different scans strategies. In (J), the biofilm-covered areas were quantitated for each group considering all scan modes. (K) The proportion of biofilm coverage is shown per each scan mode. Significant (asterisks) and non-significant (NS) differences are indicated when groups were compared. Scale bar = 1,400 µm

Figure 4 - Evaluation of *C. tropicalis* biofilm growth with WSI. (A-I) Virtual images of biofilms growing at the surface of coverslips in the control group (A-C) and after antifungal treatments (D-I) acquired with different scans strategies. In (J), the biofilm-covered areas were quantitated for each group considering all scan modes. (K) The proportion of biofilm coverage is shown per each scan mode. Significant (asterisks, $P<0.0001$) and non-significant (NS) differences are indicated when groups were compared. Scale bar = 1,400 µm

Figure 5 - Architecture of *Candida* biofilms normally growing in cultures. (A, B) *C. albicans* form a highly dense biofilm with channel-like structures (arrows) flowing through the biofilm extent. (C, D) *C. glabrata* biofilm is characterized by a meshwork shape with thin filamentous stretches of relatively small fungal cells surrounding an empty, almost round opening. (E, F) *C. tropicalis* biofilm shows a honeycomb-like chambers. WSI images were acquired under bright-field (A, C, F) or fluorescence/DAPI staining (B, D, F) modes. Scale bar, 200µm

Figure 6 – Single-cell morphology of *Candida* biofilms normally growing in cultures. (A-C) High-resolution WSI images of *C. albicans, C. glabrata* and *C. tropicalis*, respectively, observed at bright-field mode. In (D-F), the same fields are observed by WSI in fluorescence mode. In (G-I), images from scanning electron microscopy (SEM) shows the same shapes observed by WSI. (J) Cell area and (K) cell roundness were quantitated in images acquired with WSI and SEM, with no difference between these two tools. A total of 121 WSI images and 123 electron micrographs were analysed. Asterisk indicates significant difference ($P = 0.01$). Scale bar; 6 µm (A-F), 3 µm (G-I).

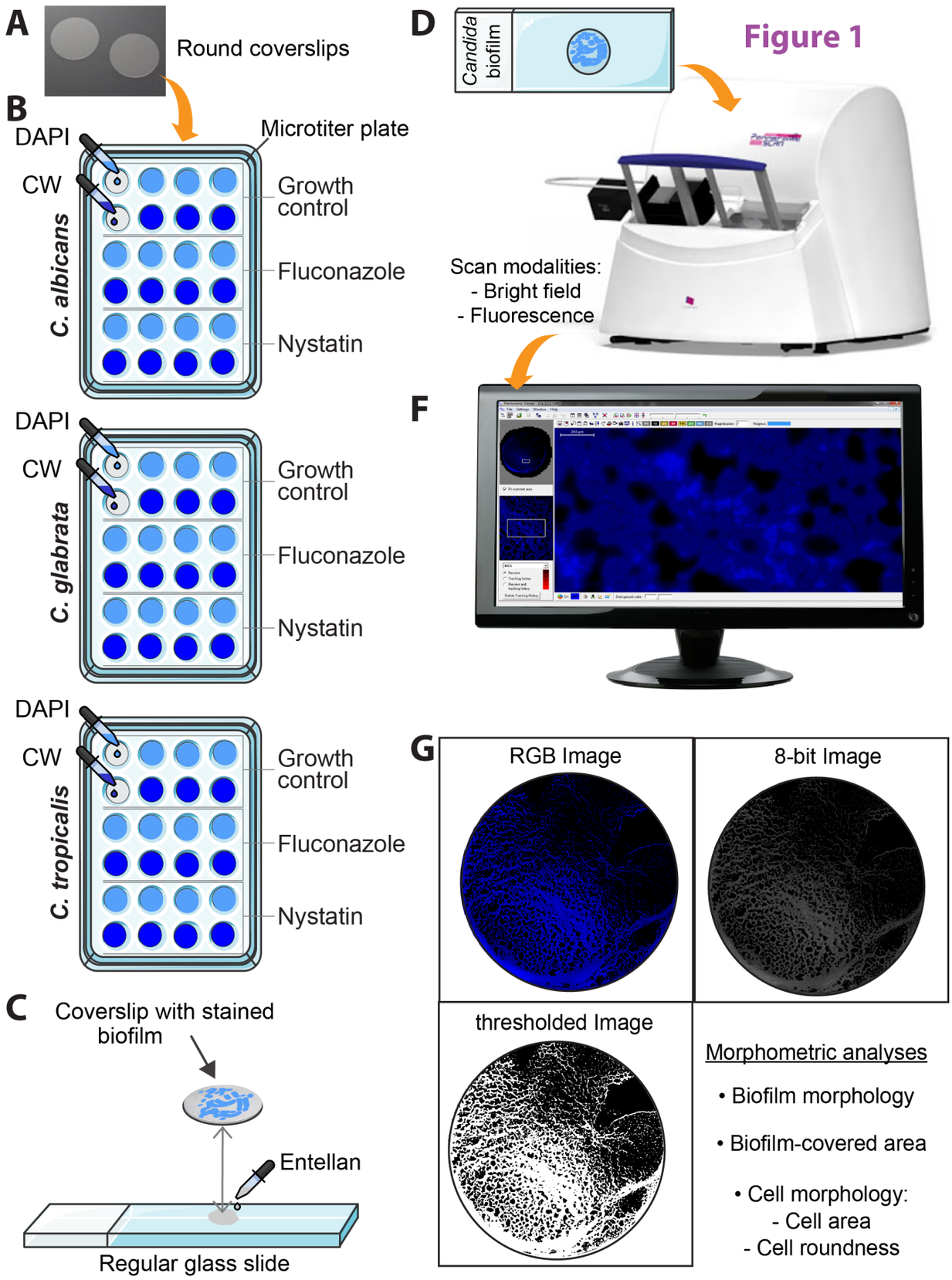
A
Round coverslips
B
DAPI
CW
Microtiter plate
Growth control
Fluconazole
Nystatin
C. albicans
C. glabrata
C. tropicalis
C
Coverslip with stained biofilm
Entellan
Regular glass slide
D
Candida biofilm
Figure 1
Scan modalities:
- Bright field
- Fluorescence
F
G
RGB Image
8-bit Image
thresholded Image
Morphometric analyses
• Biofilm morphology
• Biofilm-covered area
• Cell morphology:
- Cell area
- Cell roundness

FIGURE 2

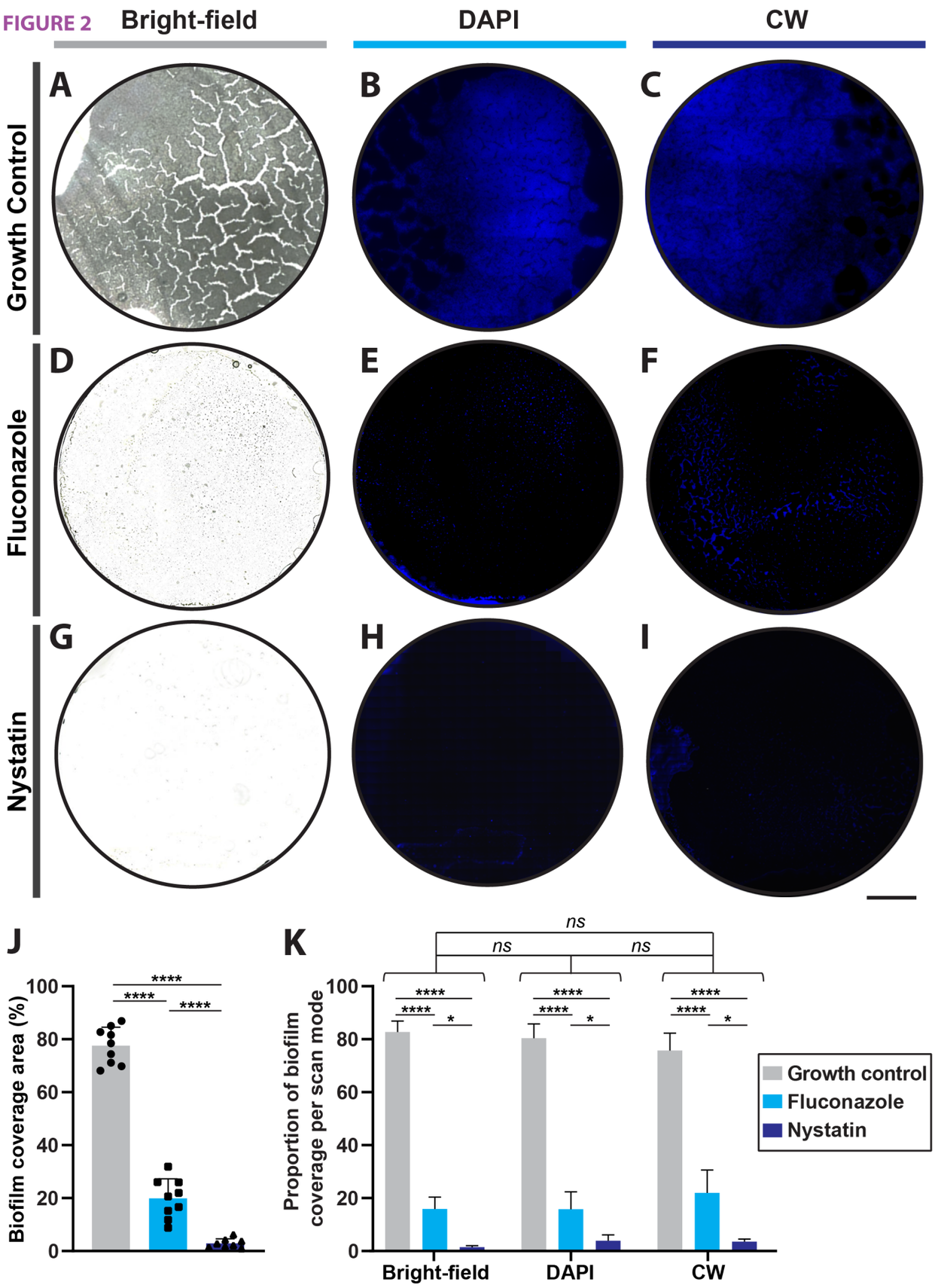
Bright-field
DAPI
CW
Growth Control
Fluconazole
Nystatin
A
B
C
D
E
F
G
H
I
J
Biofilm coverage area (%)
100
80
60
40
20
0
****
****
****
K
Proportion of biofilm coverage per scan mode
ns
ns
ns
****
****
*
Growth control
Fluconazole
Nystatin
Bright-field
DAPI
CW

FIGURE 3

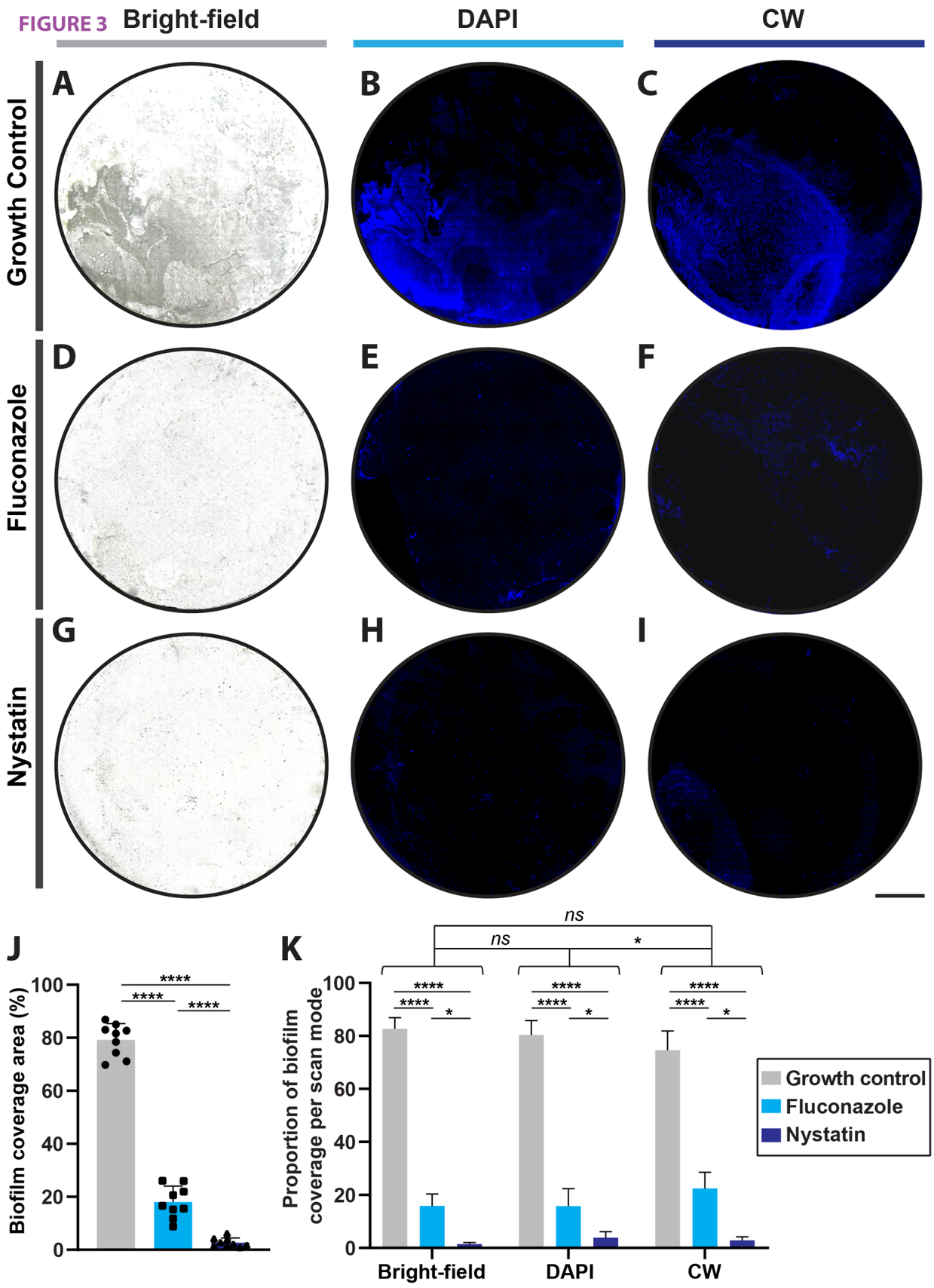
Bright-field
DAPI
CW
Growth Control
Fluconazole
Nystatin
A
B
C
D
E
F
G
H
I
J
Biofilm coverage area (%)
100
80
60
40
20
0
****
****
****
K
Proportion of biofilm coverage per scan mode
ns
ns
*
****
****
*
Growth control
Fluconazole
Nystatin
Bright-field
DAPI
CW

FIGURE 4

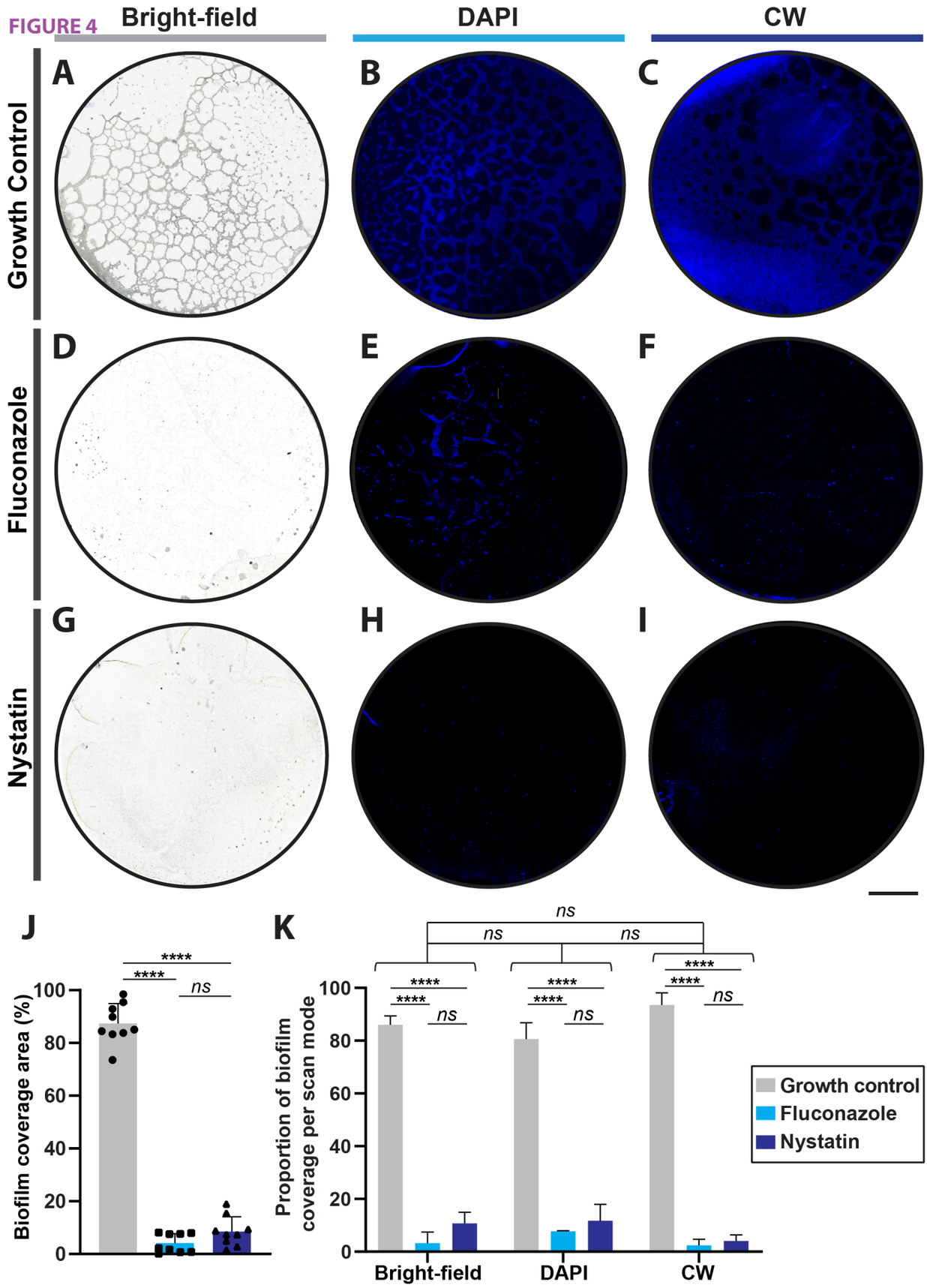
Bright-field
DAPI
CW
Growth Control
Fluconazole
Nystatin
A
B
C
D
E
F
G
H
I
J
K
Biofilm coverage area (%)
Proportion of biofilm coverage per scan mode
****
ns
Growth control
Fluconazole
Nystatin
Bright-field
DAPI
CW

FIGURE 5

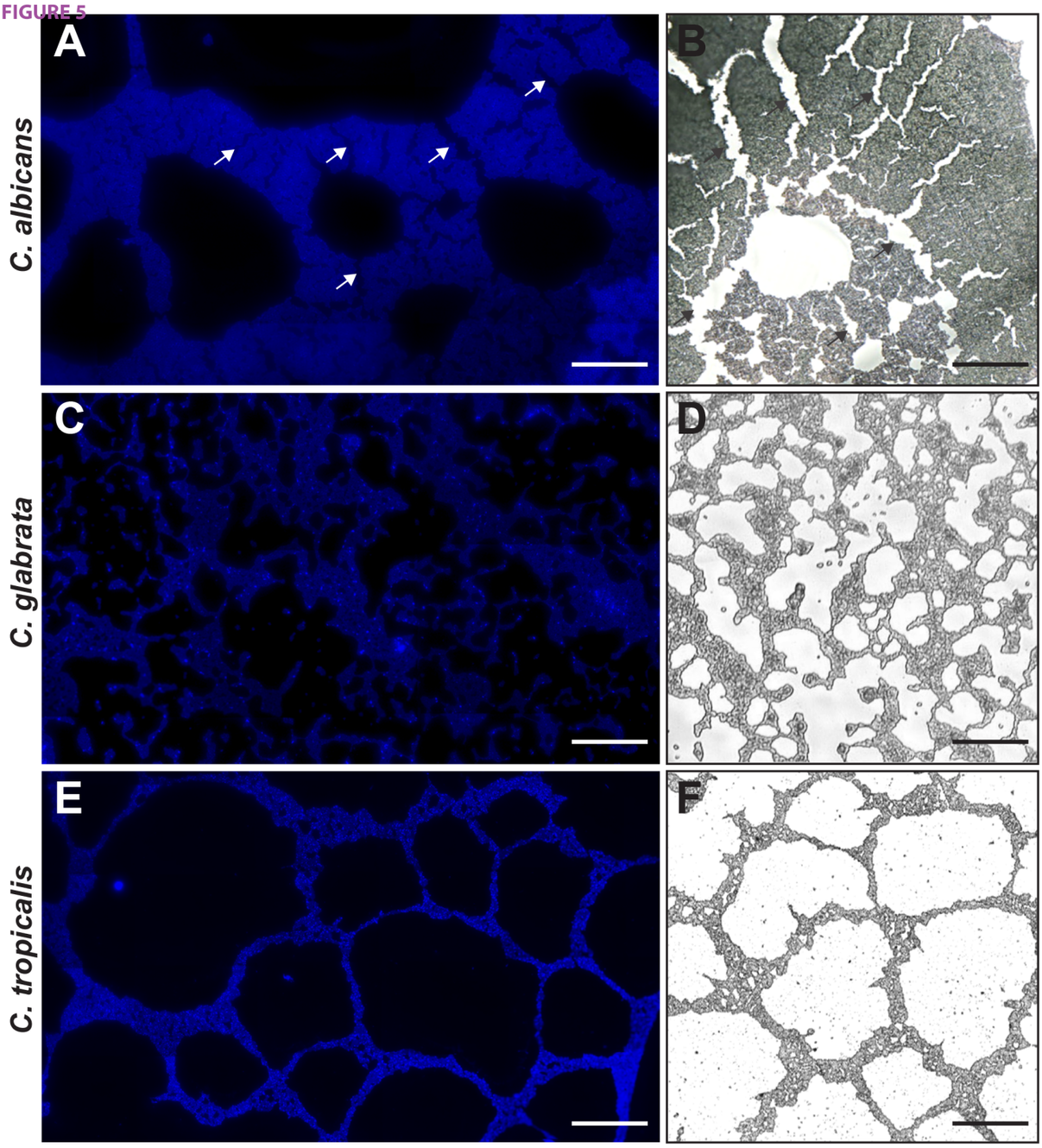

FIGURE 6

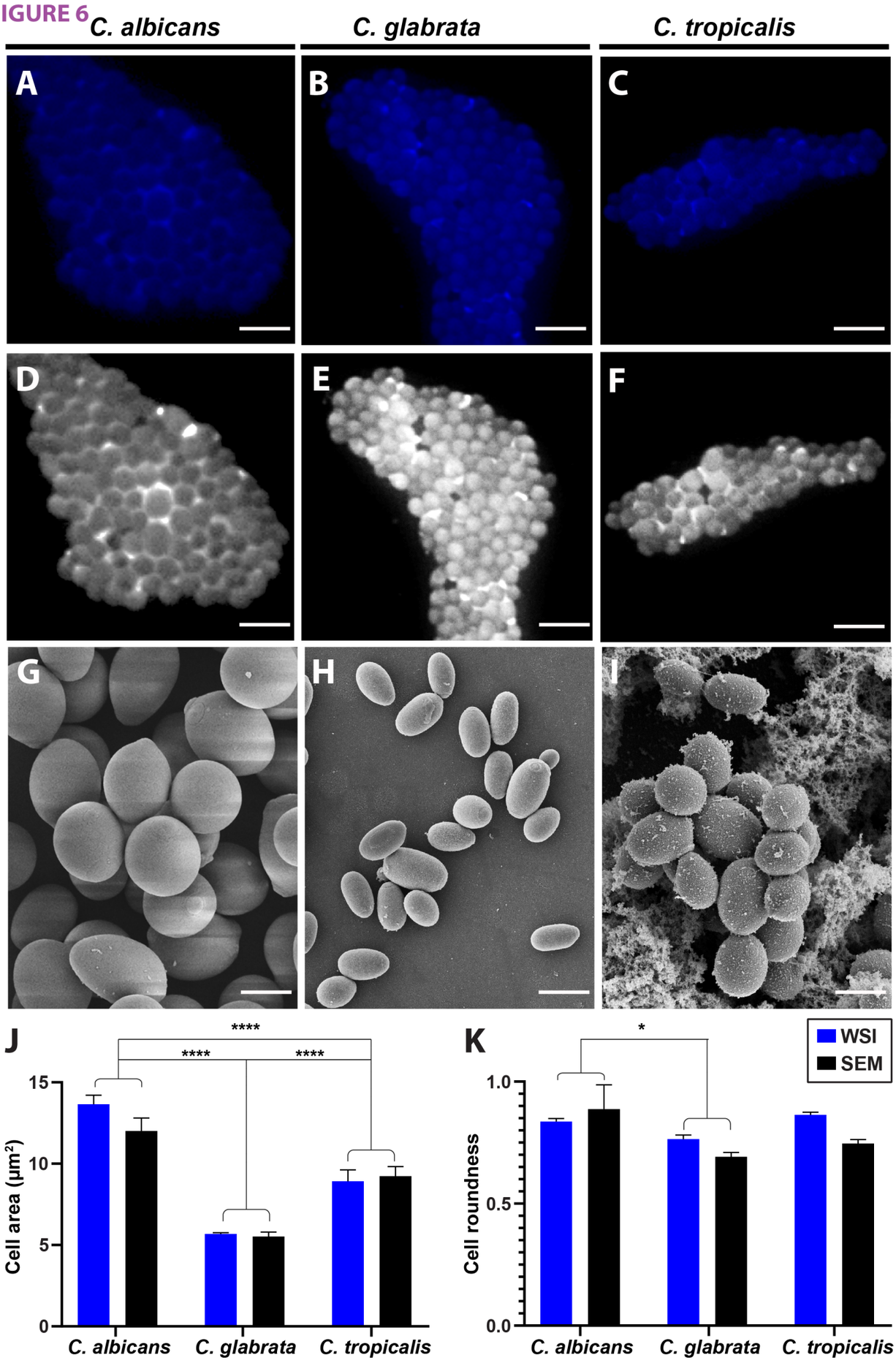
C. albicans
C. glabrata
C. tropicalis
A
B
C
D
E
F
G
H
I
J
****
****
****
15
10
5
0
Cell area (μm²)
C. albicans
C. glabrata
C. tropicalis
K
*
WSI
SEM
1.0
0.5
0.0
Cell roundness
C. albicans
C. glabrata
C. tropicalis